4-12-2021

Transient deactivation of dorsal premotor cortex or parietal area 5 impairs feedback control of the limb in macaques

Tomohiko Takei
Queen's University, Centre for Neuroscience Studies, Kingston

Stephen G. Lomber
Université McGill, steve.lomber@uwo.ca

Douglas J. Cook
Queen's University, Centre for Neuroscience Studies, Kingston

Stephen H. Scott
Queen's University, Centre for Neuroscience Studies, Kingston

Article

Current Biology

Transient deactivation of dorsal premotor cortex or parietal area 5 impairs feedback control of the limb in macaques

Highlights

- Temporary cooling of PMd and A5 distinctly impairs feedback corrections
- Effects match respective reductions of feedback and Kalman gains in control models
- Results are validated with different patterns of cooling (dual and reduced cooling)

Authors

Tomohiko Takei, Stephen G. Lomber, Douglas J. Cook, Stephen H. Scott

Correspondence

takeitomohiko@gmail.com (T.T.), steve.scott@queensu.ca (S.H.S.)

In Brief

Takei et al. demonstrate temporary cooling of premotor and parietal cortex distinctly impairs arm feedback corrections in macaque monkeys, reflecting distinct aspects of control and state estimation, respectively. These findings provide causal evidence that broad cortical areas are involved in goal-directed feedback control.

Takei et al., 2021, Current Biology *31*, 1476–1487
April 12, 2021
https://doi.org/10.1016/j.cub.2021.01.049

CellPress

CellPress

Current Biology

Article

Transient deactivation of dorsal premotor cortex or parietal area 5 impairs feedback control of the limb in macaques

Tomohiko Takei,[1,6,7,8,*] Stephen G. Lomber,[5] Douglas J. Cook,[1,4] and Stephen H. Scott[1,2,3,*]
[1]Centre for Neuroscience Studies, Queen's University, Kingston, ON K7L 3N6, Canada
[2]Department of Biomedical and Molecular Sciences, Queen's University, Kingston, ON K7L 3N6, Canada
[3]Department of Medicine, Queen's University, Kingston, ON K7L 3N6, Canada
[4]Department of Surgery, Division of Neurosurgery, Queen's University, Kingston, ON K7L 3N6, Canada
[5]Department of Physiology, McGill University, Montreal, QC H3G 1Y6, Canada
[6]Graduate School of Medicine, Kyoto University, Kyoto 606-8501, Japan
[7]The Hakubi Center for Advanced Research, Kyoto University, Kyoto 606-8501, Japan
[8]Lead contact
*Correspondence: takeitomohiko@gmail.com (T.T.), steve.scott@queensu.ca (S.H.S.)
https://doi.org/10.1016/j.cub.2021.01.049

SUMMARY

We can generate goal-directed motor corrections with surprising speed, but their neural basis is poorly understood. Here, we show that temporary cooling of dorsal premotor cortex (PMd) impaired both spatial accuracy and the speed of corrective responses, whereas cooling parietal area 5 (A5) impaired only spatial accuracy. Simulations based on optimal feedback control (OFC) models demonstrated that "deactivation" of the control policy (reduction in feedback gain) and state estimation (reduction in Kalman gain) caused impairments similar to that observed for PMd and A5 cooling, respectively. Furthermore, combined deactivation of both cortical regions led to additive impairments of individual deactivations, whereas reducing the amount of cooling to PMd led to impairments in response speed but not spatial accuracy, both also predicted by OFC models. These results provide causal support that frontoparietal circuits beyond primary somatosensory and motor cortices are involved in generating goal-directed motor corrections.

INTRODUCTION

A hallmark of our voluntary motor system is the ability to generate goal-directed motor corrections. This can be as simple as stabilizing a water bottle when filling it from a tap to as complex as maintaining balance when someone bumps you on a crowded subway platform while simultaneously moving a cup of hot coffee away from your body to avoid being scalded.

Optimal feedback control (OFC) is a powerful normative model for understanding how the motor system ought to respond to noise and disturbances in performance.[1–5] These controllers include two key processes: (1) an optimal control policy that flexibly generates motor commands based on task goals and system state (position and motion of the body), and (2) optimal state estimation that uses efference copy of motor commands and sensory feedback to estimate system state. These models capture a broad range of behavioral features of motor performance including the ability to generate variable, but successful, movements[6] and goal-directed motor corrections that consider myriad factors such as limb mechanics, target redundancy, urgency, and the presence of obstacles.[3,7–12]

How our CNS generates these goal-directed motor corrections is poorly understood. It has been commonly assumed that goal-directed motor corrections are generated principally through a rapid transcortical pathway involving primary somatosensory (S1) and primary motor cortex (M1), leading to muscle responses in as little as 60 ms for the proximal arm.[5,13,14] However, our recent study highlighted that short latency neural responses can be observed across frontoparietal circuits in monkeys when mechanical disturbances are applied to the forelimb in as little as 25 ms, including in higher order motor (dorsal premotor cortex, PMd) and somatosensory regions (parietal area 5, A5)[15]. This observation suggests that the generation of rapid feedback responses may involve broader frontoparietal circuits, normally associated with motor planning and initiation.[16–18]

The objective of this study is to provide physiological and computational support that these cortical regions are causally involved in goal-directed feedback control by quantifying how transient deactivation of each cortical region, induced with cortical cooling,[19,20] impacts goal-directed feedback control. We begin with OFC models to explore how disruption or "deactivation" of different processes impacts feedback control. These reverse engineering approaches have been used in previous studies to successfully dissect motor control processes.[21,22] In the present study, we find that reductions in gains associated with different processes lead to distinct patterns of impairments to counter mechanical disturbances when maintaining a fixed spatial position. Observed impairments generated by cooling PMd and/or A5 in monkeys also generated distinct patterns of

impairments in feedback control that paralleled impairments associated with the control policy and state estimate in OFC, respectively. These results provide causal support that broad frontoparietal circuits are involved in goal-directed feedback control, and localized disruption in this circuit generates distinct patterns of impairments.

RESULTS

OFC model predictions

How could changes in a feedback circuit alter goal-directed feedback responses? We made theoretical predictions for the motor deficits that may occur from deactivating a brain region using a stochastic optimal feedback control (OFC) model (Figure 1A).[1,23] Although other models of the motor system exist, such as feedback error learning[24,25] and active inference,[26,27] we use OFC as a general model of the motor system because it captures the highly flexible nature of biological control, does not require a desired trajectory like the former, and can manage sensory and motor delays unlike the latter.

We first optimized model parameters to reproduce the monkey's intact feedback response (Figure 1B). Then, we applied deactivation to the model parameters (Figure 1A), including (1) the feedback gain (L) of the control policy, (2) Kalman gain (K) in state estimation, (3) parameters in the internal forward model ($\hat{A}$, $\hat{B}$, and $\hat{H}$), and (4) the sensory observation matrix (H). Because cooling reduces neural excitability in adjacent tissue,[19] we modeled a cooling effect as a reduction of each parameter (for a different deactivation method based on increases in noise, see "Alternate deactivation model based on cooling increasing neural noise"). First, large reductions in any parameter ultimately led to failure of the model to generate appropriate motor corrections to mechanical disturbances (Figure 1D). Of particular interest is that smaller reductions of parameters led to unique patterns of feedback impairments for each parameter (Figures 1C and 1D). Reduction of the feedback gain (L), that converts estimates of system state into motor commands, generates a broad range of impairments, including reduction in spatial accuracy (endpoint error) and several metrics related to response speed (return time, max deviation, and max deviation time) (Figures 1C and 1D, red; $p < 0.05$). Reduction of Kalman gain (K) degrades the use of external sensory feedback, making state estimation more reliant on internal feedback. This generated impairments in spatial accuracy (endpoint error), but interestingly, did not impair response speed (return time and max deviation time) until the gain was reduced more than ~60% (Figures 1C and 1D, blue; $p > 0.05$). This reflects that reduction of the Kalman gain induces only a small delay in updating the state estimation about the presence of a perturbation using external sensory feedback, but once updated, internal feedback can then appropriately counter the external perturbation. Even small reductions of parameters in the internal forward model ($\hat{A}$, $\hat{B}$, and $\hat{H}$) providing internal feedback for state estimation quickly leads to severe oscillations ($\hat{A}$, Figure 1C, green; $\hat{B}$ and $\hat{H}$, Figure S1A), with rapid degradation in spatial accuracy (Figures 1D, green, and S1B; $p < 0.05$) . Finally, reduction of the sensory observation matrix (H) degrades sensory information. This generated severe impairments in spatial accuracy and response speed (Figures 1C and 1D, orange; $p < 0.05$), qualitatively similar to impairments associated with the feedback gain (L). Taken together, our simulations highlight that deactivation of different model parameters generates unique patterns, or signatures, of motor impairments that can be used to dissociate cortical functions.

Impact of PMd and A5 cooling on feedback corrections

The traditional view is that frontal motor cortex is involved in "motor" processing and parietal cortex is involved in "sensory" processing.[16,18,28] Thus, we hypothesized that PMd cooling would cause parallel impairments associated with reductions in the feedback gain (spatial accuracy and response times) and A5 cooling would cause parallel impairments associated with the Kalman gain (only spatial accuracy).

To test our hypotheses, we chronically implanted cooling probes over the surface of PMd and A5 (Figure 2A). By circulating chilled methanol through the probes, we are able to cool down the cortical temperature and deactivate each area[19] while observing changes in motor performance during a single experimental session reversibly and temporarily (Figure 2B). Monkeys were trained to maintain their fingertip at a central target and to make corrections to mechanical perturbations unexpectedly applied to the forelimb (posture perturbation task, Figure 2C). On separate days, the task was performed before (pre-cool), during (cool), and after cooling (post-cool) of each cortical region, including sham controls when cooling was not applied (monkey A: PMd n = 23, A5 n = 31, sham n = 28; monkey R: PMd n = 10, A5 n = 18, sham n = 51 sessions).

When PMd was cooled, motor responses were slowed (Figure 3A, bottom, circles) and response accuracy was reduced (Figure 3A, top, squares), resulting in a significant increase in endpoint errors ($t[79.7] = 4.8$, $p < 0.05$) (Figure 3C) and response speed (return time, max deviation, and max deviation time, $t[87.2] = 5.7$, $t[83.8] = 4.4$, $t[88.1] = 5.4$, $p < 0.05$, respectively). Correspondingly, the muscle stretch response was reduced beginning in the long-latency time epoch (R3 epoch, 75–120 ms after perturbation onset, $t[92.3] = 3.6$, $p < 0.05$) (Figure 3D), which is the first instance that transcortical feedback can contribute to feedback corrections.[12–14,29] These results are consistent with our hypothesis that PMd cooling impairs the feedback control policy. These behavioral effects were consistent between two load conditions (SE+EE and SF+EF) with some differences, such as a continued change in endpoint error after A5 cooling only in SF+EE load (Figure S2). We also confirmed that these behavioral effects were consistent between two monkeys with some individual variations in effect size (Figure S3). Importantly, we confirmed that these effects were not induced by the direct cooling of M1 (Figure 4). In monkey A, we implanted a chamber over M1 and recorded intracortical temperature by inserting a thermocouple needle into the arm area of M1 (PMd cooling, n = 2, dual PMd and A5 cooling, n = 1). We found that a change of M1 temperature was minimal (<2°C) and higher than the cortical temperature that suppresses neural activity (<20°C).[19]

When A5 was cooled, the endpoint variability was increased similarly to the PMd cooling (Figure 3B, top, squares). However, in contrast to PMd cooling, during A5 cooling monkey was still able to return to the target quickly within 500 ms (Figure 3B,

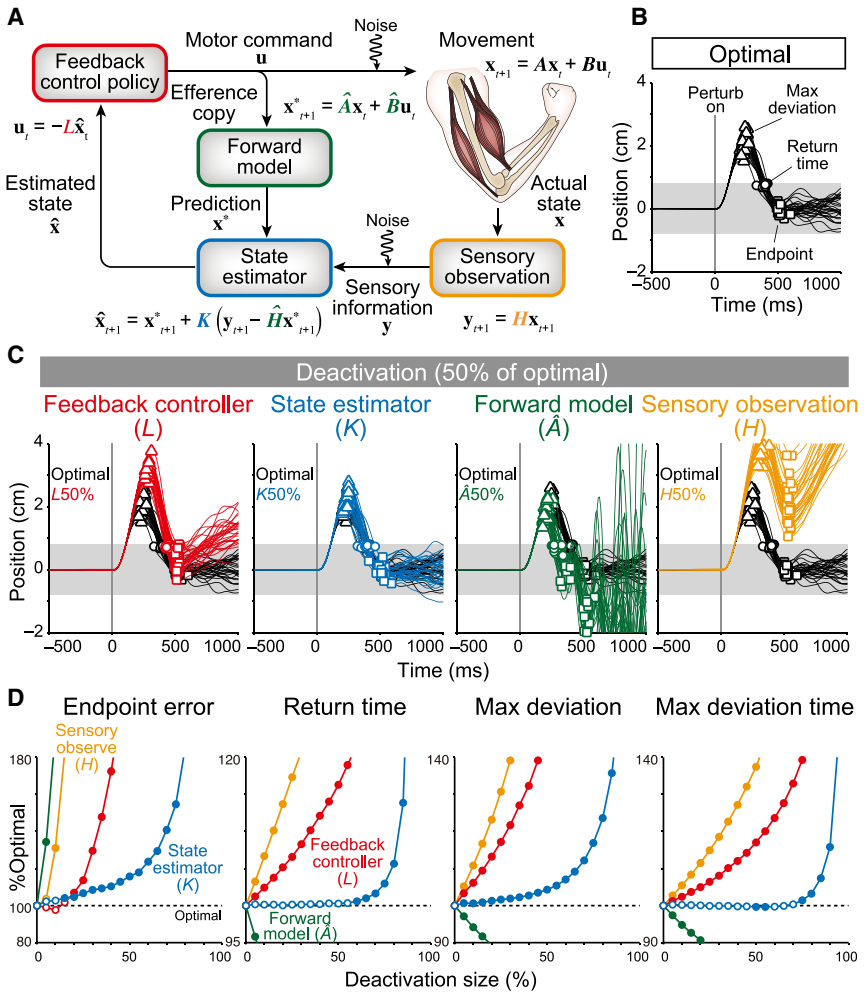

Figure 1. OFC model predictions

(A) Optimal feedback control model.

(B) Response of the model to mechanical perturbations in optimized condition.

(C) Response of the model in deactivated conditions. Black lines denote the optimized condition (same to B). Colored lines denote trials when each parameter was reduced by 50%. Red, feedback gain in feedback controller (*L*); blue, Kalman gain (*K*) in state estimator; green, a parameter of forward model ($\hat{A}$); orange, observation matrix in sensory observation (*H*).

(D) Performance measures impaired by the deactivation of model parameters. All measures showed significant interaction and main effects in a two-way ANOVA (deactivation size × deactivated parameters), suggesting unique patterns of motor impairments for each parameter ($p < 0.05$). Filled circles, significant difference from optimal condition (t test, $p < 0.05$).

See also Figure S1.

bottom, circles). These results were confirmed by significant increase in endpoint errors ($t[162] = 5.3$, $p < 0.05$, Figure 3C), but no significant change in parameters of response speed (return time, max deviation, and max deviation time, $t[200] = 0.4$, $t[162] = 0.4$, and $t[201] = 1.4$, $p > 0.5$, respectively). This result suggests that although spatial accuracy was impaired, the ability to generate the rapid motor response was preserved during A5 cooling. This was confirmed by the lack of significant changes in EMG during the R3 epoch during A5 cooling ($t[63] = 1.8$, $p = 0.42$, Figure 3E). These results are consistent with the results of deactivation of Kalman gain (*K*) in the state estimation where spatial accuracy was impaired but not response speed, supporting our hypothesis that A5 cooling impairs state estimation.

Simultaneous cooling of PMd and A5 emulates deactivation of feedback control gain and Kalman gain

Because our simulation showed that reductions of feedback control gain (*L*) and sensory observation matrix (*H*) caused qualitatively similar effects (Figure 1D), we could not separate whether PMd cooling impaired feedback gain or sensory observation. Therefore, we further dissociate their effects by simulating the simultaneous cooling of PMd and A5 with a simultaneous reduction of *L* and *K* (*L* & *K*), or *H* and *K* (*H* & *K*). Figure 5A shows the results of simultaneous reduction of *L* & *K*. The top panels show the impairment of each performance measure as a function of deactivation of *L* (horizontal axis) with different size of deactivation *K* (different colors). As expected, the size of impairments was increased as deactivation size was increased. To highlight the difference of the effects between the different deactivation size of *K*, the effect in *K*100% condition (0% deactivation of *K*) was subtracted from each plot (difference from *K*100%, Figure 5A, bottom row). The result shows that plots are mostly flat or slightly decreasing, indicating that simultaneous reduction of *L* & *K* led to impairments that were a linear sum or a sublinear interaction of impairments for each parameter separately (Figure 5A). In contrast, when we tested the interaction between the deactivation of *H* and *K*, the impairments become larger than the linear summation of impairments induced by each parameter (Figure 5B). These results indicate simultaneous reduction of *H* & *K* caused supralinear interaction of impairments.

To test the interaction of the effect of PMd and A5 cooling, we simultaneously cooled PMd and A5 (n = 20 and 10 in monkey A and R, Figure 6A, "Dual"). The result showed that impairments were a linear sum (endpoint error, return time, and max deviation time) or a trend of the sublinear interaction (max deviation) of impairments induced by individual cooling of each area separately (Figure 6A, "Sum"; endpoint error, return time, and max deviation time, $t[59] = 0.7$, $t[59] = 0.1$, and $t[59] = 0.3$, $p > 0.9$, respectively; max deviation, $t[59] = 1.2$, $p = 0.47$). These behavioral effects were consistently observed between two monkeys (Figure S4). Importantly, these results are qualitatively similar to the effects of the simultaneous cooling of *L* & *K* (Figure 5A). These results provide further support for our hypotheses that PMd and A5 are

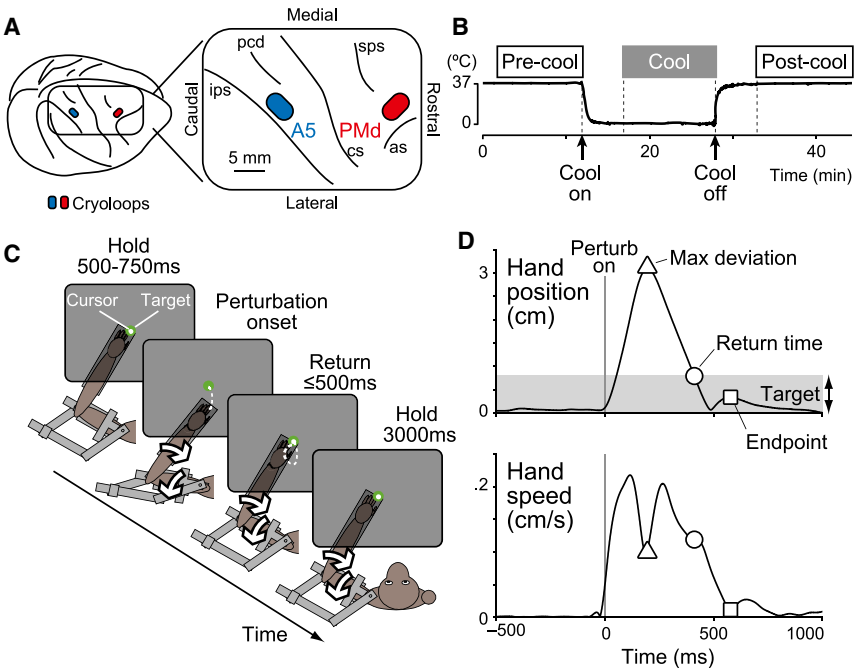

Figure 2. Experimental setups for cortical cooling

(A) Cooling probes were implanted over dorsal premotor cortex (PMd) and parietal area 5 (A5) in the right hemisphere of monkeys. as, arcuate sulcus; cs, central sulcus; ips, intraparietal sulcus; pcd, postcentral dimple; sps, superior precentral sulcus.

(B) Feedback motor responses were tested before (pre-cool), during (cool), and after (post-cool) cooling.

(C) Postural perturbation task. Monkey must maintain its hand at a central target. A mechanical load was applied to the limb and the monkey must return its hand to the same spatial target in less than 500 ms and maintain its hand for another 3 s.

(D) Hand position and speed in an exemplar trial. Symbols denote behavioral measures: max deviation (triangle), return time (circle), and endpoint (square).

involved with the feedback control policy (*L*) and state estimation (*K*), respectively.

Milder cooling of PMd selectively impacts speed of motor corrections

We further tested a prediction obtained from the model. Our simulation of deactivation of the feedback gain *L* (Figure 1D, red) showed that although a larger reduction of *L* induced the impairment of all measures, a small reduction in *L* ($\leq$20%) would lead to a unique pattern of impairments in which all parameters, but not endpoint error, would be impaired (e.g., 10% deactivation of *L* in Figure 1D). Therefore, we predicted that if PMd cooling impaired the feedback gain *L*, the milder deactivation of PMd impaired all measurements but endpoint error. We tested this prediction by applying milder cooling of PMd in one animal (8°C instead of 1°C in probe temperature, n = 5 in monkey R). Results showed that milder cooling of PMd significantly impaired all parameters (return time, max deviation, and max deviation time, $t[11] = 3.2$, $t[10] = 3.3$, and $t[10] = 4.0$, $p < 0.05$, respectively) except endpoint errors (Figure 6B, pink, $t[12] = 0.8$, $p = 1.0$). This result further validates our hypothesis that PMd cooling impaired feedback gain *L* of feedback responses.

Alternate deactivation model based on cooling increasing neural noise

In addition to downscaling, we also simulated the effect of cortical cooling by adding scaled Gaussian noise to each OFC parameter (see STAR methods). This method was based on an assumption that cortical cooling deactivates a population of excitatory and inhibitory neurons that increases noise in the gain rather than unidirectionally downscaling neural gain. Results showed that the noise addition produced qualitatively similar effects on behavioral parameters to the downscaling (Figures 1 versus 7). First, noise addition to feedback gain (*L*) impaired both spatial accuracy (endpoint error) and response speed (return time), whereas noise addition to Kalman gain (*K*) impaired the endpoint error but less for return time at smaller deactivations (10%–30% coefficient of variation). Second, noise addition to forward models ($\hat{A}$, $\hat{B}$, $\hat{H}$) led to severe oscillations. Last, noise addition to sensory observation matrix (*H*) impaired both spatial accuracy and response speed (max deviation and max deviation time).

It is noteworthy, however, that there were some discrepancies between simulation results with noise addition and cortical cooling. First, the max deviation and max deviation time was less impaired by noise addition to feedback gain (*L*) or Kalman gain (*K*). This is inconsistent with the results of PMd cooling, where all these parameters were significantly impaired (Figure 3C). Second, a smaller noise addition to feedback gain (*L*) was not able to predict the results of milder cooling of PMd (8°C in probe temperature), which impaired response speed but not spatial accuracy. Although both mechanisms (reduction of gain and increase of noise) might underlie the effect of cortical cooling, the downscaling of model parameters appears to be a better model to explain the effects of cortical cooling.

DISCUSSION

In this study, we combined deactivation experiments applied with cortical cooling and simulations based on an OFC model to examine the contributions of PMd and A5 on online feedback control. The results highlight that deactivation of PMd impaired both spatial accuracy and response speed, whereas deactivation of A5 impaired spatial accuracy, but not response speed (Figure 3), indicating their causal involvement to the generation of feedback motor corrections. Correspondingly, simulations based on optimal feedback control (OFC) model demonstrated that deactivation of the control policy (reduction of feedback gain *L*) impaired both spatial accuracy and response speed, whereas deactivation in state estimation (reduction of Kalman

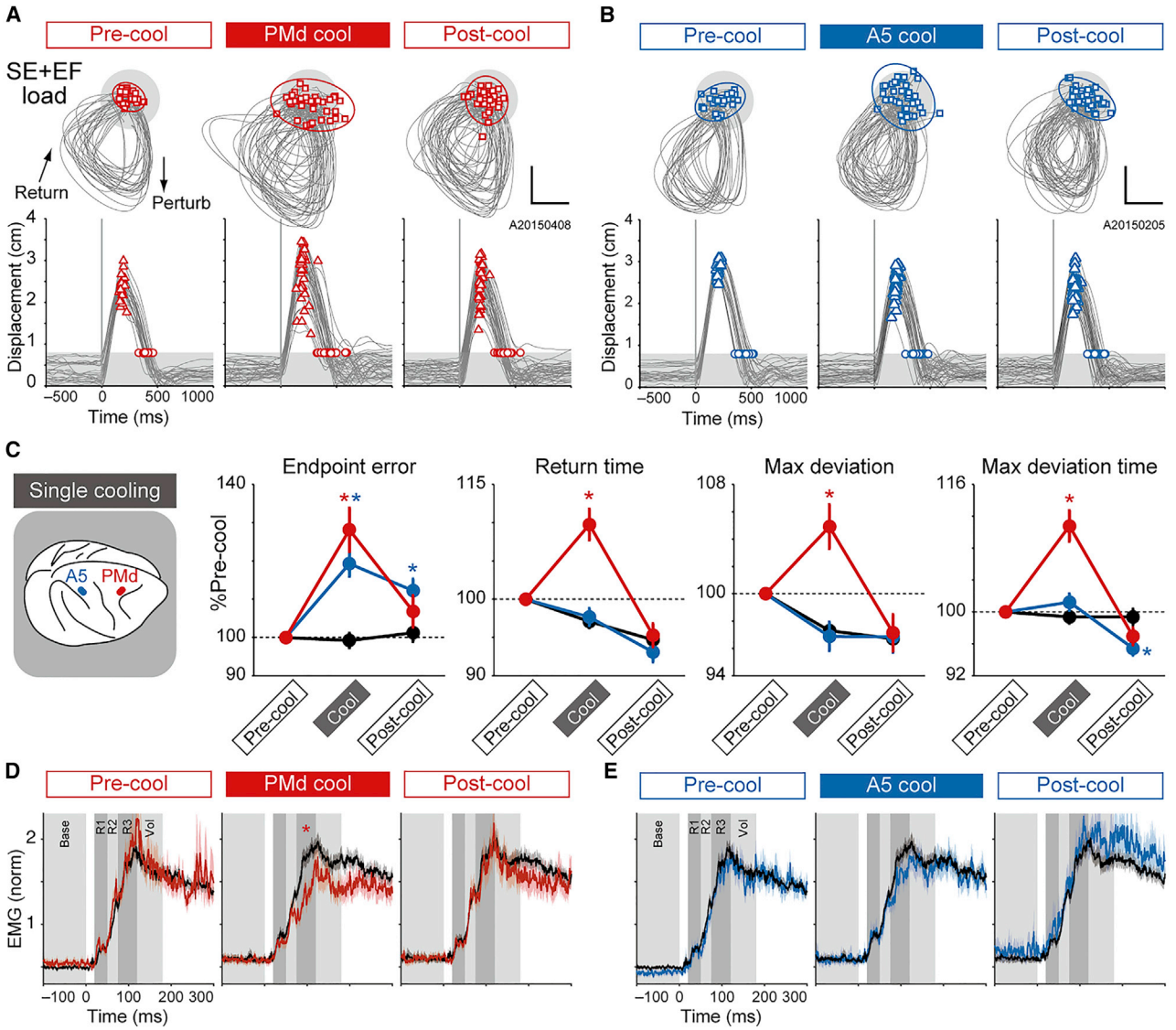

Figure 3. Impact of PMd and A5 cooling on feedback corrections

(A and B) Hand trajectories (top) and hand displacements (bottom) when the limb was unexpectedly perturbed with a shoulder extension and elbow flexion (SE+EF) load in pre-cool, cool, and post-cool PMd conditions (A) and corresponding A5 conditions (B). Calibration bars, 1 cm. Ellipses, 95% confident interval of endpoints. Time = 0, perturbation onset.

(C) Performance measures for PMd (red), A5 (blue), and sham (black) cooling sessions. Averages across two monkeys and two torque directions after normalized to pre-cool condition. Error bars, SEM. All measures displayed significant interaction and main effects in a two-way ANOVA (cooling epochs × target areas) indicating different effects of cortical cooling ($p < 0.05$). *Significant difference from sham condition (t test, $p < 0.05$).

(D and E) Averaged EMG responses to mechanical perturbations in PMd (red), A5 (blue), and sham (black) cooling sessions. Responses were binned to baseline (100–0 ms before perturbation), R1 (20–50 ms post-perturbation), R2 (50–75 ms), R3 (75–120 ms), and voluntary (120–180 ms) time windows (gray and dark gray rectangles). Shaded areas, SEM. *Significant difference from sham condition (t test, $p < 0.05$).

See also Figures S2 and S3.

gain *K*) impaired spatial accuracy but not response speed (Figure 1), paralleling the impairments observed from deactivation of PMd and A5, respectively. Furthermore, simultaneous deactivation of PMd and A5 led to additive impairments of individual deactivations (Figure 6A), whereas milder cooling of PMd led to impairments in response speed, but not spatial accuracy (Figure 6B). Again, the OFC model predicted both of these observations. These results clearly support our hypothesis that PMd and A5 are causally involved in goal-directed feedback control: the corresponding patterns of impairment suggest distinct roles related to the control policy and state estimation, respectively.

Control models predict a variety of motor impairments

Many studies show how disruption or alteration of motor circuits can lead to complex impairments in motor performance.[30–37] For example, genetic ablation of cervical propriospinal neurons,

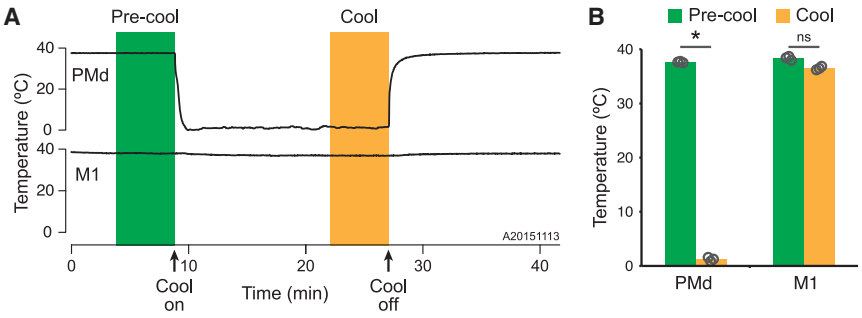

Figure 4. PMd and M1 temperature changes during PMd cooling

(A) Example of cortical temperature measured from M1 during a PMd cooling experiment. Cooling probe on PMd was cooled to 1°C and the probe temperature was measured (top). An independent thermocouple was acutely inserted to M1 arm area (bottom).

(B) Averaged temperature of PMd probe and M1 in pre-cool and cool epochs of PMd only (n = 2) and dual PMd and A5 cooling (n = 1). *Significant difference between pre-cool and cool conditions (t test, $p < 0.05$). ns, non-significant. Note that during PMd cooling or dual cooling, a change of M1 temperature was minimal (<2°C) and did not reach significant limit.

projecting to brainstem pre-cerebellar nucleus, causes severe oscillations during reaching whereas locomotion and posture control are intact.[34] As well, disruption of thalamocortical activity prevents movement initiation or halts ongoing movement,[35] and cooling in dentate nucleus causes oscillations or tremor during reaching and when responding to mechanical perturbations.[36,37] Why does disruption of motor circuits lead to such complex motor impairments?

We used a formal control model to interpret how disruption of key processes impacts motor corrections. We used a stochastic optimal feedback control model because this has been a common normative model for interpreting motor behavior for the last 15 years.[1,2,5,38] We expect qualitatively similar results would be observed for other control models that possess a control policy and state estimation that integrates internal and external sensory feedback, known features of the voluntary motor system.[39–42] Our model was initially optimized to generate feedback corrections that matched the speed and accuracy observed for the monkeys prior to cooling. Notable in Figure 1 is how a small reduction in an optimized parameter can lead to minimal or profound impairments in performance. For example, even a 10% reduction in parameters related to the forward model ($\hat{A}$) leads to extremely poor control, and larger reductions lead to instability (Figures 1C and 1D, green). This requirement to have a very accurate forward model is a known challenge with stochastic OFC.[43] Other control frameworks, such as robust control, help to mitigate this problem by considering the potential presence of systematic errors in the model[44,45] and such models capture certain features on how humans move, and in particular, deal with unexpected disturbances and adaptation to novel loads.[41,46]

Perhaps the most surprising pattern of impairment was predicted for the Kalman gain where reductions up to 50% largely impacted only endpoint error and not the speed of the correction (return time and max deviation time, Figure 1D, blue). The Kalman gain is the weighting between internal feedback provided by a forward model based on efference copy and external sensory feedback from the limb or other sensory modalities: a smaller value means the model relies more on internal feedback (x^* in Figure 1A). Intuitively, one might assume that the corrective response should be delayed when relying less on external sensory feedback as well as increasing the endpoint error. However, when the Kalman gain was reduced, only increases in endpoint error were observed in the model. The simple explanation is that a reduction in the Kalman gain induces only a small delay in updating the presence of a perturbation that must be sensed from external sensory feedback, but once updated, internal feedback from the forward model can appropriately counter the external perturbation. Endpoint errors do increase with a reduced (i.e., suboptimal) Kalman gain, because one must continuously adjust motor commands for noise in the system. This highlights how alterations in control parameters can generate unexpected changes in performance. Note that our simulation used a point mass model that will not capture features such as intersegmental interaction where there is a difference between joint motion and the applied torques.[7,29] However, this should not really impact the general properties of speed and accuracy of corrective responses, which was the focus of the present study.

It is also noteworthy that the reductions in return time and max deviation were observed whether cortical cooling was applied or not (sham, Figure 3C, black circles) and reflect a general change in the performance of the animals with time during a behavioral session. In contrast, endpoint error and max deviation time showed differences from the sham condition after A5 cooling (Figure 3C) and suggest some changes in performance remained after cooling was stopped. This can be also observed as a slight increase of EMG after A5 cooling (Figure 3E). This may suggest that the motor system was trying to adapt during the cooling period, and that is an interesting issue warranting further investigation.

Interpreting computations in brain circuits based on OFC

The use of OFC or other formal control models provide a way of understanding the complex relationship between specific control processes and motor performance. OFC has been commonly used as a normative model to describe motor function at the behavioral level and captures many aspects of human motor performance including successful movements with a high trial-to-trial variability[47,48] and goal-directed modulation of feedback responses to mechanical perturbation of the limb according to shape and location of the spatial goal,[10,49] features of the environment,[8,11] and urgency of the response.[50]

The mathematical techniques associated with OFC are certainly not performed by the motor system, but general processes related to a control policy and state estimation including forward models capture many behavioral aspects of the motor

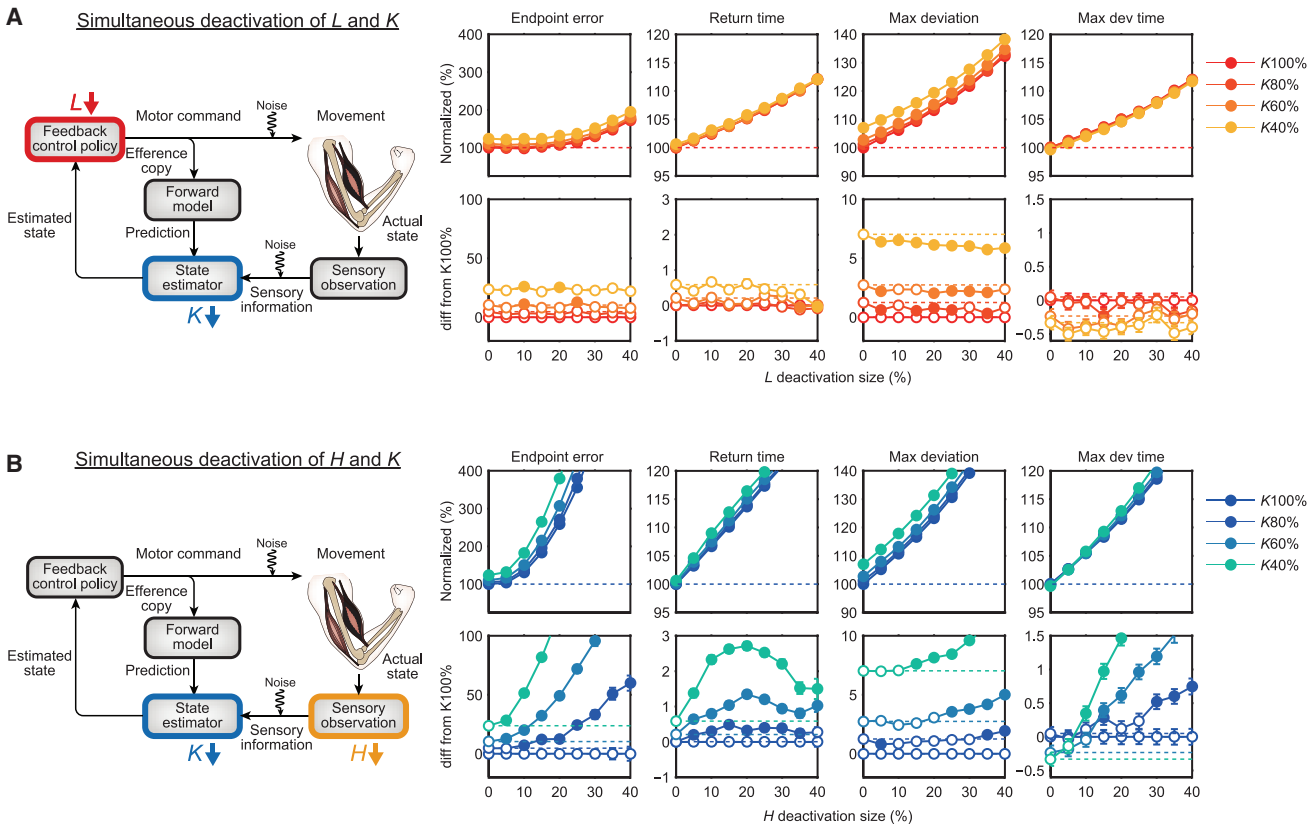

Figure 5. Simulation of the effect of dual deactivations

(A and B) Results for dual deactivation of feedback gain and Kalman gain (*L* & *K*, A) and observation matrix and Kalman gain (*H* & *K*, B). Top: performance measures were normalized to the optimal condition (dashed line). Bottom: difference from the *K*100% condition (0% deactivation of *K*). Horizontal dashed lines denote the linear sum of the deactivation of parameters (*L* & *K* or *H* & *K*). Filled circle, significant difference from the linear sum (t test, $p < 0.05$). Note that the effects are linear or sublinear for *L* & *K* deactivation, whereas they are supralinear for *H* & *K*.

system.[4,5,12,40] However, directly applying these control processes to motor circuits is not straightforward. Motor circuits that support online control are highly distributed, including many cortical and subcortical regions. Many different regions likely contribute to each process, and a single brain region may participate in multiple processes.[38] Thus, it is highly unlikely that a single brain region is exclusively responsible for a single parameter or control process.

For example, the control policy in which motor commands are generated based on the present state of the body likely involves cortical, brainstem, and spinal processing, because each level contributes to a certain degree to the final pattern of muscle activity during a motor action. The final motor command only emerges at the motoneuronal level (the final common path)[51] as some descending projections synapse directly onto motoneurons.[52] This distributed and hierarchical organization means that the contribution at the highest cortical level will not simply reflect the pattern of muscle activity for a motor action. Thus, temporary deactivation in any of these brain regions involved in feedback control could lead to impairments that look like a reduction in control policy gains.

What is perhaps surprising is that deactivation of PMd leads to impairments that parallel those for reductions in control policy gains, because this cortical region is normally associated with motor planning rather than motor execution.[53–55] Evidence to support its role in motor planning come from the large body of research, such as delayed reaching tasks, in which neural activity increases in PMd when the monkey has been instructed on the location of a spatial goal.[56–61] In contrast, M1 is associated with motor execution and online control, because this motor cortical region displays less preparatory activity but displays substantive activity during movement execution.[57,59–61]

There are at least two explanations as to why deactivation of PMd leads to patterns of impairment that match that associated with a control policy. First, PMd has strong projections to M1, brainstem, and spinal cord.[62–64] Thus, deactivation in this cortical region indirectly impacts feedback performance by altering other regions that are part of the control policy.[38] Alternatively, PMd may be more directly involved in online control. Previous work highlights that this brain region responds in as little as 25 ms to mechanical disturbances of the limb, and this pattern of activity is altered based on behavioral context.[15] Although PMd certainly displays preparatory activity prior to movement, it also displays substantial activity during movement execution.[56–61] Recent studies highlight how neural activity during preparatory period can be maintained in a

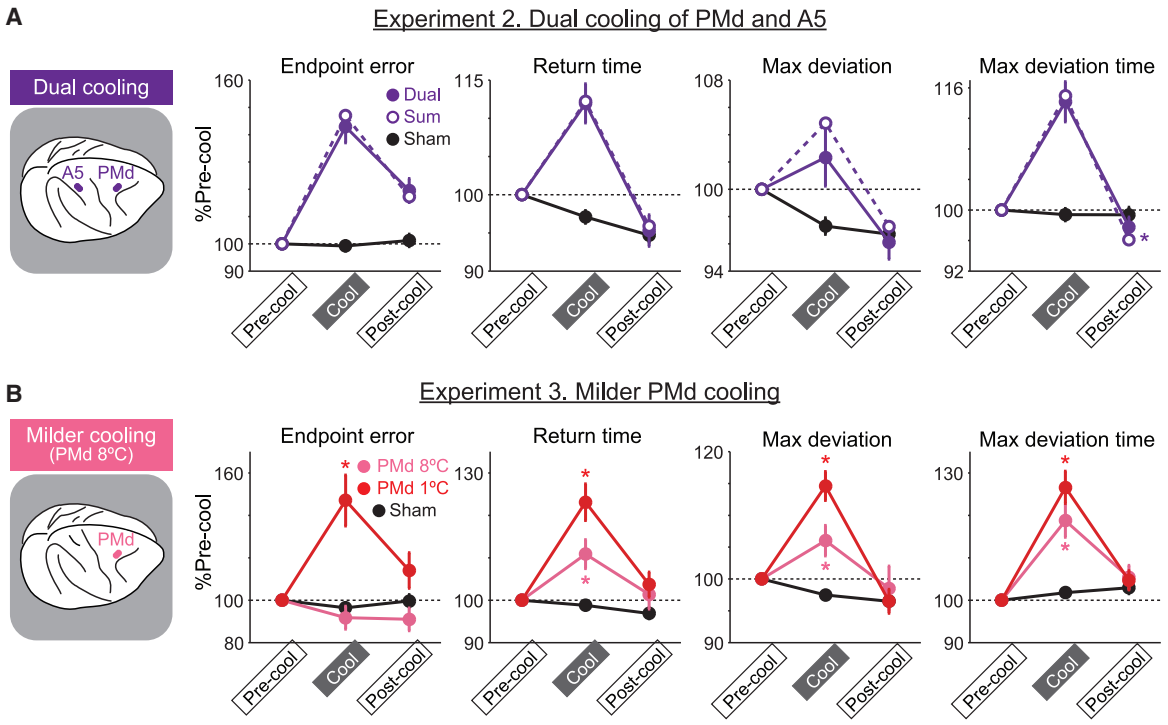

Figure 6. Effects of dual cooling and milder PMd cooling

(A) Performance measures of dual cooling of PMd and A5 (filled circle, "Dual") were compared with a linear summation of the effects of single PMd and A5 cooling (open circle, "Sum"). *Significant difference between dual cooling and linear sum (t test, $p < 0.05$).

(B) Comparison of original cooling (1°C in probe temperature, red) and milder cooling of PMd (8°C, pink). *Significant difference from sham condition (t test, $p < 0.05$). Error bars, SEM. All measures showed significant interaction and main effects in a two-way ANOVA (cooling epochs × target areas) indicating different effects of cortical cooling ($p < 0.05$).

See also Figure S4.

neural subspace such that it does not influence motor output. After a "go" cue, this activity shifts to another subspace that can influence motor output.[65–67] It is possible that PMd could simultaneously be involved in motor planning in one subspace, while it also contributes to online feedback control in another orthogonal subspace.

As a higher somatosensory region, A5 has traditionally been associated with body representations for sensation and voluntary control.[68] Many studies demonstrate lesions or deactivation of this area cause sensorimotor deficits associating with the impairment in voluntary control.[69–73] The present study found temporary deactivation in A5 led to impairments in rapid motor corrections for mechanical perturbation of the limb that were qualitatively similar to those expected for reductions in the Kalman gain (i.e., increase of endpoint error but no change of return time). As with the control policy, the Kalman gain likely involves many cortical and subcortical regions. However, temporary deactivation in this cortical region appears to be sufficient to disrupt this key process, again directly by impacting activity within A5 and/or indirectly through its influence in other sensorimotor regions.

It is also interesting to note that reductions in parameters associated with the forward model led to large errors even for small reductions in gain and even oscillatory behavior for reductions at ~50% (Figures 1C and S1A). Accumulating evidence supports a role of the cerebellum for forward models in motor control[74–79]. The forward model is essential to make a prediction of the state to overcome sensorimotor delays that can destabilize control[39,80]. Our results demonstrate that relatively small errors in the forward model can induce undesirable oscillatory behavior. Interestingly, the oscillatory behavior we observed resembles ataxia of cerebellar patients and a pattern of impairment when the dentate nucleus in the cerebellum was cooled[36,37]. These results provide mechanistic explanation for the emergence of cerebellar ataxia.

Limitations of study

There are clear limitations in comparing OFC models to our cooling experiments on monkeys. Notably, it is not possible to know how cooling in a brain region should be compared to the amount of reduction in a given control parameter. We nominally compared our behavioral results to 50% reductions in the control parameters. However, the pattern of impairment for reductions in the Kalman gain are reasonably stable for reductions between 20%–60%; values less than this range lead to minimal effects, whereas greater values lead to both speed and accuracy errors. Reductions in control policy gain were also fairly stable from 20%–50% with both speed and accuracy being affected. Cooling in a cortical region never entirely stopped the monkey's ability to generate goal-directed responses during cortical cooling. The first possible explanation is that the cooling impacted a limited region of PMd or A5. Although a previous study showed

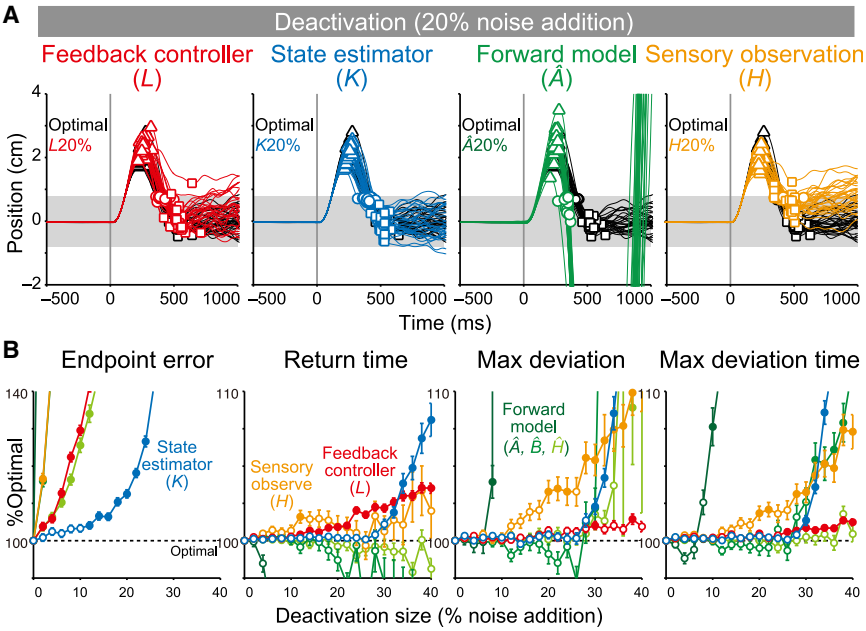

Figure 7. Alternate deactivation model based on cooling increasing neural noise

(A) Response of the model when a scaled Gaussian noise (20% coefficient of variation) was added to each parameter. Same format as Figure 1C.

(B) Impairment of behavioral measures as a function of deactivation size. Filled circles, significant difference from optimal condition (t test, $p < 0.05$). Note that this noise addition method produced largely similar effects to the downscaling (Figure 1). First, noise addition to feedback gain (L) impaired both spatial accuracy (endpoint error) and response speed (return time), whereas noise addition to Kalman gain (K) impaired the endpoint error but less effect on response speed at smaller deactivation size (10%–30% coefficient of variation). Second, noise addition to forward models ($\hat{A}$, $\hat{B}$, $\hat{H}$) led severe oscillations. Finally, noise addition to sensory observation matrix (H) impaired both spatial accuracy and response speed (max deviation and max deviation time).

that the cortical cooling silences almost all postsynaptic activity in the cooled region,[19] it is possible that our cooling did not affect the entire cortical territory, such as deeper regions of a sulcus. Second, other regions may also contribute to that specific process in a parallel manner. For example, M1, which is almost certainly involved in processes associated with the control policy[5,13,14,29,81], was still active with PMd cooling and likely contributes to a control policy. Further studies exploring this issue by recording in regions such as M1 when PMd or A5 is cooled are warranted.

In many ways, it is surprising that 50% reductions of some gains only lead to small impairments in control. Further, the patterns of impairments change as the gain is reduced, and impairments can have linear or non-linear interactions depending on the components that are disrupted. Our follow-up experiments (i.e., dual cooling and milder cooling) exploited these complex features of control providing testable predictions. Thus, intuition is not sufficient to interpret the behavior of a dynamical system like our motor system and demonstrates the need for control models to aid interpretation. Although OFC models proved useful for cortical circuits, more biological-inspired hierarchical models will likely be necessary to interpret how the disruption of brainstem and spinal circuits impact control.

STAR★METHODS

Detailed methods are provided in the online version of this paper and include the following:

SUPPLEMENTAL INFORMATION

Supplemental information can be found online at https://doi.org/10.1016/j.cub.2021.01.049.

ACKNOWLEDGMENTS

We thank Kim Moore, Simone Appaqaq, Justin Peterson, Helen Bretzke, and Mike Lewis for their laboratory and technical assistance; Dr. Mohsen Omrani for his support to setup the cooling system; Dr. Frédéric Crevecoeur for his support to model the OFC simulation; and members of the LIMB lab for constructive discussion. This work was supported by the Canadian Institutes of Health Research (CIHR), Grants-in-Aid (19H03975, 19H05311) from the Ministry of Education, Culture, Sports, Science and Technology of Japan (MEXT), the Uehara Memorial Foundation, the Naito Foundation, and the Takeda Science Foundation.

AUTHOR CONTRIBUTIONS

Conceptualization, T.T. and S.H.S.; Methodology, T.T., S.G.L., D.J.C., and S.H.S.; Investigation, T.T.; Writing – Original Draft, T.T. and S.H.S.;

Writing – Review & Editing, T.T., S.G.L., D.J.C., and S.H.S.; Funding Acquisition, S.H.S.; Supervision, S.H.S.

DECLARATION OF INTERESTS

S.H.S. is co-founder and Chief Scientific Officer of Kinarm that commercializes the robotic technology used in this study and holds several related patents.

Received: November 6, 2020
Revised: January 13, 2021
Accepted: January 13, 2021
Published: February 15, 2021

REFERENCES

1. Todorov, E., and Jordan, M.I. (2002). Optimal feedback control as a theory of motor coordination. Nat. Neurosci. *5*, 1226–1235.
2. Scott, S.H. (2004). Optimal feedback control and the neural basis of volitional motor control. Nat. Rev. Neurosci. *5*, 532–546.
3. Franklin, D.W., and Wolpert, D.M. (2008). Specificity of reflex adaptation for task-relevant variability. J. Neurosci. *28*, 14165–14175.
4. Diedrichsen, J., Shadmehr, R., and Ivry, R.B. (2010). The coordination of movement: optimal feedback control and beyond. Trends Cogn. Sci. *14*, 31–39.
5. Scott, S.H., Cluff, T., Lowrey, C.R., and Takei, T. (2015). Feedback control during voluntary motor actions. Curr. Opin. Neurobiol. *33*, 85–94.
6. Liu, D., and Todorov, E. (2007). Evidence for the flexible sensorimotor strategies predicted by optimal feedback control. J. Neurosci. *27*, 9354–9368.
7. Kurtzer, I.L., Pruszynski, J.A., and Scott, S.H. (2008). Long-latency reflexes of the human arm reflect an internal model of limb dynamics. Curr. Biol. *18*, 449–453.
8. Shemmell, J., An, J.H., and Perreault, E.J. (2009). The differential role of motor cortex in stretch reflex modulation induced by changes in environmental mechanics and verbal instruction. J. Neurosci. *29*, 13255–13263.
9. Knill, D.C., Bondada, A., and Chhabra, M. (2011). Flexible, task-dependent use of sensory feedback to control hand movements. J. Neurosci. *31*, 1219–1237.
10. Nashed, J.Y., Crevecoeur, F., and Scott, S.H. (2012). Influence of the behavioral goal and environmental obstacles on rapid feedback responses. J. Neurophysiol. *108*, 999–1009.
11. Nashed, J.Y., Crevecoeur, F., and Scott, S.H. (2014). Rapid online selection between multiple motor plans. J. Neurosci. *34*, 1769–1780.
12. Scott, S.H. (2016). A Functional Taxonomy of Bottom-Up Sensory Feedback Processing for Motor Actions. Trends Neurosci. *39*, 512–526.
13. Evarts, E.V., and Tanji, J. (1976). Reflex and intended responses in motor cortex pyramidal tract neurons of monkey. J. Neurophysiol. *39*, 1069–1080.
14. Cheney, P.D., and Fetz, E.E. (1984). Corticomotoneuronal cells contribute to long-latency stretch reflexes in the rhesus monkey. J. Physiol. *349*, 249–272.
15. Omrani, M., Murnaghan, C.D., Pruszynski, J.A., and Scott, S.H. (2016). Distributed task-specific processing of somatosensory feedback for voluntary motor control. eLife *5*, e13141.
16. Shadmehr, R., and Wise, S.P. (2005). The Computational Neurobiology of Reaching and Pointing: A Foundation for Motor Learning (MIT Press).
17. Andersen, R.A., and Cui, H. (2009). Intention, action planning, and decision making in parietal-frontal circuits. Neuron *63*, 568–583.
18. Rizzolatti, G., and Kalaska, J.F. (2013). Voluntary movement: the parietal and premotor cortex. In Principles of Neural Science, Fifth Edition (McGraw Hill Professional), pp. 1–29.
19. Lomber, S.G., Payne, B.R., and Horel, J.A. (1999). The cryoloop: an adaptable reversible cooling deactivation method for behavioral or electrophysiological assessment of neural function. J. Neurosci. Methods *86*, 179–194.
20. Payne, B.R., and Lomber, S.G. (1999). A method to assess the functional impact of cerebral connections on target populations of neurons. J. Neurosci. Methods *86*, 195–208.
21. Benyamini, M., and Zacksenhouse, M. (2015). Optimal feedback control successfully explains changes in neural modulations during experiments with brain-machine interfaces. Front. Syst. Neurosci. *9*, 71.
22. Mathis, M.W., Mathis, A., and Uchida, N. (2017). Somatosensory Cortex Plays an Essential Role in Forelimb Motor Adaptation in Mice. Neuron *93*, 1493–1503.e6.
23. Todorov, E. (2005). Stochastic optimal control and estimation methods adapted to the noise characteristics of the sensorimotor system. Neural Comput. *17*, 1084–1108.
24. Kawato, M., Furukawa, K., and Suzuki, R. (1987). A hierarchical neural-network model for control and learning of voluntary movement. Biol. Cybern. *57*, 169–185.
25. Kawato, M. (1990). Feedback-error-learning neural network for supervised motor learning. In Advanced Neural Computers, R. Eckmiller, ed. (North-Holland), pp. 365–372.
26. Friston, K. (2010). The free-energy principle: a unified brain theory? Nat. Rev. Neurosci. *11*, 127–138.
27. Friston, K. (2011). What is optimal about motor control? Neuron *72*, 488–498.
28. Schaffelhofer, S., and Scherberger, H. (2016). Object vision to hand action in macaque parietal, premotor, and motor cortices. eLife *5*, 6436.
29. Pruszynski, J.A., Kurtzer, I., Nashed, J.Y., Omrani, M., Brouwer, B., and Scott, S.H. (2011). Primary motor cortex underlies multi-joint integration for fast feedback control. Nature *478*, 387–390.
30. Machado, A.S., Marques, H.G., Duarte, D.F., Darmohray, D.M., and Carey, M.R. (2020). Shared and specific signatures of locomotor ataxia in mutant mice. eLife *9*, 18.
31. Schieber, M.H., and Poliakov, A.V. (1998). Partial inactivation of the primary motor cortex hand area: effects on individuated finger movements. J. Neurosci. *18*, 9038–9054.
32. Stepniewska, I., Gharbawie, O.A., Burish, M.J., and Kaas, J.H. (2014). Effects of muscimol inactivations of functional domains in motor, premotor, and posterior parietal cortex on complex movements evoked by electrical stimulation. J. Neurophysiol. *111*, 1100–1119.
33. Brochier, T., Boudreau, M.J., Paré, M., and Smith, A.M. (1999). The effects of muscimol inactivation of small regions of motor and somatosensory cortex on independent finger movements and force control in the precision grip. Exp. Brain Res. *128*, 31–40.
34. Azim, E., Jiang, J., Alstermark, B., and Jessell, T.M. (2014). Skilled reaching relies on a V2a propriospinal internal copy circuit. Nature *508*, 357–363.
35. Sauerbrei, B.A., Guo, J.-Z., Cohen, J.D., Mischiati, M., Guo, W., Kabra, M., Verma, N., Mensh, B., Branson, K., and Hantman, A.W. (2020). Cortical pattern generation during dexterous movement is input-driven. Nature *577*, 386–391.
36. Meyer-Lohmann, J., Conrad, B., Matsunami, K., and Brooks, V.B. (1975). Effects of dentate cooling on precentral unit activity following torque pulse injections into elbow movements. Brain Res. *94*, 237–251.
37. Hore, J., and Flament, D. (1986). Evidence that a disordered servo-like mechanism contributes to tremor in movements during cerebellar dysfunction. J. Neurophysiol. *56*, 123–136.
38. Scott, S.H. (2012). The computational and neural basis of voluntary motor control and planning. Trends Cogn. Sci. *16*, 541–549.
39. Wolpert, D.M., and Ghahramani, Z. (2000). Computational principles of movement neuroscience. Nat. Neurosci. *3 (Suppl)*, 1212–1217.
40. Shadmehr, R., and Krakauer, J.W. (2008). A computational neuroanatomy for motor control. Exp. Brain Res. *185*, 359–381.

41. Crevecoeur, F., Scott, S.H., and Cluff, T. (2019). Robust Control in Human Reaching Movements: A Model-Free Strategy to Compensate for Unpredictable Disturbances. J. Neurosci. *39*, 8135–8148.

42. Bian, T., Wolpert, D.M., and Jiang, Z.-P. (2020). Model-Free Robust Optimal Feedback Mechanisms of Biological Motor Control. Neural Comput. *32*, 562–595.

43. Miall, R.C., Weir, D.J., Wolpert, D.M., and Stein, J.F. (1993). Is the cerebellum a smith predictor? J. Mot. Behav. *25*, 203–216.

44. Zhou, K., Doyle, J.C., and Glover, K. (1996). Robust and Optimal Control (Prentice Hall).

45. Başar, T., and Bernhard, P. (2008). H-Infinity Optimal Control and Related Minimax Design Problems (Springer Science & Business Media).

46. Cluff, T., Crevecoeur, F., and Scott, S.H. (2019). Tradeoffs in optimal control capture patterns of human sensorimotor control and adaptation. bioRxiv. https://doi.org/10.1101/730713.

47. Messier, J., and Kalaska, J.F. (1999). Comparison of variability of initial kinematics and endpoints of reaching movements. Exp. Brain Res. *125*, 139–152.

48. van Beers, R.J., Haggard, P., and Wolpert, D.M. (2004). The role of execution noise in movement variability. J. Neurophysiol. *91*, 1050–1063.

49. Pruszynski, J.A., Kurtzer, I., and Scott, S.H. (2008). Rapid motor responses are appropriately tuned to the metrics of a visuospatial task. J. Neurophysiol. *100*, 224–238.

50. Crevecoeur, F., Kurtzer, I., Bourke, T., and Scott, S.H. (2013). Feedback responses rapidly scale with the urgency to correct for external perturbations. J. Neurophysiol. *110*, 1323–1332.

51. Sherrington, S.C.S. (1906). The Integrative Action of the Nervous System (Yale University Press).

52. Fetz, E.E., Perlmutter, S.I., Prut, Y., and Maier, M.A. (1999). Primate spinal interneurons: muscle fields and response properties during voluntary movement. Prog. Brain Res. *123*, 323–330.

53. Wise, S.P. (1985). The primate premotor cortex fifty years after Fulton. Behav. Brain Res. *18*, 79–88.

54. Wise, S.P. (1985). The primate premotor cortex: past, present, and preparatory. Annu. Rev. Neurosci. *8*, 1–19.

55. Wise, S.P., Boussaoud, D., Johnson, P.B., and Caminiti, R. (1997). Premotor and parietal cortex: corticocortical connectivity and combinatorial computations. Annu. Rev. Neurosci. *20*, 25–42.

56. Weinrich, M., and Wise, S.P. (1982). The premotor cortex of the monkey. J. Neurosci. *2*, 1329–1345.

57. Weinrich, M., Wise, S.P., and Mauritz, K.H. (1984). A neurophysiological study of the premotor cortex in the rhesus monkey. Brain *107*, 385–414.

58. Kurata, K. (1993). Premotor cortex of monkeys: set- and movement-related activity reflecting amplitude and direction of wrist movements. J. Neurophysiol. *69*, 187–200.

59. Crammond, D.J., and Kalaska, J.F. (2000). Prior information in motor and premotor cortex: activity during the delay period and effect on pre-movement activity. J. Neurophysiol. *84*, 986–1005.

60. Cisek, P., Crammond, D.J., and Kalaska, J.F. (2003). Neural activity in primary motor and dorsal premotor cortex in reaching tasks with the contralateral versus ipsilateral arm. J. Neurophysiol. *89*, 922–942.

61. Nakayama, Y., Yamagata, T., and Hoshi, E. (2016). Rostrocaudal functional gradient among the pre-dorsal premotor cortex, dorsal premotor cortex and primary motor cortex in goal-directed motor behaviour. Eur. J. Neurosci. *43*, 1569–1589.

62. Kuypers, H.G.J.M. (1981). Anatomy of the descending pathways. In The Nervous System, Handbook of Physiology, Vol. 2, V. Brooks, ed. (Williams and Wilkins), pp. 597–666.

63. Wiesendanger, M. (1981). Organization of secondary motor areas of cerebral cortex. In Handbook of Physiology: The Nervous System, *Vol. 13* (American Cancer Society), pp. 1121–1147.

64. Dum, R.P., and Strick, P.L. (1991). The origin of corticospinal projections from the premotor areas in the frontal lobe. J. Neurosci. *11*, 667–689.

65. Kaufman, M.T., Churchland, M.M., Ryu, S.I., and Shenoy, K.V. (2014). Cortical activity in the null space: permitting preparation without movement. Nat. Neurosci. *17*, 440–448.

66. Elsayed, G.F., Lara, A.H., Kaufman, M.T., Churchland, M.M., and Cunningham, J.P. (2016). Reorganization between preparatory and movement population responses in motor cortex. Nat. Commun. *7*, 13239.

67. Perich, M.G., Gallego, J.A., and Miller, L.E. (2018). A Neural Population Mechanism for Rapid Learning. Neuron *100*, 964–976.e7.

68. Head, H., and Holmes, G. (1911). Sensory disturbances from cerebral lesions. Brain *34*, 102–254.

69. Wolpert, D.M., Goodbody, S.J., and Husain, M. (1998). Maintaining internal representations: the role of the human superior parietal lobe. Nat. Neurosci. *1*, 529–533.

70. Desmurget, M., Epstein, C.M., Turner, R.S., Prablanc, C., Alexander, G.E., and Grafton, S.T. (1999). Role of the posterior parietal cortex in updating reaching movements to a visual target. Nat. Neurosci. *2*, 563–567.

71. Pisella, L., Gréa, H., Tilikete, C., Vighetto, A., Desmurget, M., Rode, G., Boisson, D., and Rossetti, Y. (2000). An 'automatic pilot' for the hand in human posterior parietal cortex: toward reinterpreting optic ataxia. Nat. Neurosci. *3*, 729–736.

72. Prablanc, C., Desmurget, M., and Gréa, H. (2003). Neural control of on-line guidance of hand reaching movements. Prog. Brain Res. *142*, 155–170.

73. Battaglia-Mayer, A., Ferrari-Toniolo, S., Visco-Comandini, F., Archambault, P.S., Saberi-Moghadam, S., and Caminiti, R. (2013). Impairment of online control of hand and eye movements in a monkey model of optic ataxia. Cereb. Cortex *23*, 2644–2656.

74. Wolpert, D.M., Miall, R.C., and Kawato, M. (1998). Internal models in the cerebellum. Trends Cogn. Sci. *2*, 338–347.

75. Blakemore, S.J., Frith, C.D., and Wolpert, D.M. (2001). The cerebellum is involved in predicting the sensory consequences of action. Neuroreport *12*, 1879–1884.

76. Nowak, D.A., Timmann, D., and Hermsdörfer, J. (2007). Dexterity in cerebellar agenesis. Neuropsychologia *45*, 696–703.

77. Miall, R.C., Christensen, L.O.D., Cain, O., and Stanley, J. (2007). Disruption of state estimation in the human lateral cerebellum. PLoS Biol. *5*, e316.

78. Izawa, J., Criscimagna-Hemminger, S.E., and Shadmehr, R. (2012). Cerebellar contributions to reach adaptation and learning sensory consequences of action. J. Neurosci. *32*, 4230–4239.

79. Zimmet, A.M., Cao, D., Bastian, A.J., and Cowan, N.J. (2020). Cerebellar patients have intact feedback control that can be leveraged to improve reaching. eLife *9*, e53246.

80. Crevecoeur, F., and Scott, S.H. (2013). Priors engaged in long-latency responses to mechanical perturbations suggest a rapid update in state estimation. PLoS Comput. Biol. *9*, e1003177.

81. Pruszynski, J.A., Omrani, M., and Scott, S.H. (2014). Goal-dependent modulation of fast feedback responses in primary motor cortex. J. Neurosci. *34*, 4608–4617.

82. Scott, S.H. (1999). Apparatus for measuring and perturbing shoulder and elbow joint positions and torques during reaching. J. Neurosci. Methods *89*, 119–127.

83. Herter, T.M., Korbel, T., and Scott, S.H. (2009). Comparison of neural responses in primary motor cortex to transient and continuous loads during posture. J. Neurophysiol. *101*, 150–163.

84. Scott, S.H., Sergio, L.E., and Kalaska, J.F. (1997). Reaching movements with similar hand paths but different arm orientations. II. Activity of individual cells in dorsal premotor cortex and parietal area 5. J. Neurophysiol. *78*, 2413–2426.

85. Coderre, A.M., Zeid, A.A., Dukelow, S.P., Demmer, M.J., Moore, K.D., Demers, M.J., Bretzke, H., Herter, T.M., Glasgow, J.I., Norman, K.E., et al. (2010). Assessment of upper-limb sensorimotor function of subacute stroke patients using visually guided reaching. Neurorehabil. Neural Repair *24*, 528–541.

86. Kurtzer, I., Pruszynski, J.A., Herter, T.M., and Scott, S.H. (2006). Primate upper limb muscles exhibit activity patterns that differ from their anatomical action during a postural task. J. Neurophysiol. *95*, 493–504.

87. Omrani, M., Pruszynski, J.A., Murnaghan, C.D., and Scott, S.H. (2014). Perturbation-evoked responses in primary motor cortex are modulated by behavioral context. J. Neurophysiol. *112*, 2985–3000.

88. Brown, I.E., Cheng, E.J., and Loeb, G.E. (1999). Measured and modeled properties of mammalian skeletal muscle. II. The effects of stimulus frequency on force-length and force-velocity relationships. J. Muscle Res. Cell Motil. *20*, 627–643.

89. Crevecoeur, F., Sepulchre, R.J., Thonnard, J.L., and Lefèvre, P. (2011). Improving the state estimation for optimal control of stochastic processes subject to multiplicative noise. Automatica *47*, 591–596.

90. Brooks, V.B. (1983). Study of brain function by local, reversible cooling. Rev. Physiol. Biochem. Pharmacol. *95*, 1–109.

STAR★METHODS

KEY RESOURCES TABLE

REAGENT or RESOURCE	SOURCE	IDENTIFIER
Experimental models: organisms/strains		
Rhesus macaque (Macaca mulatta)	Queen's University	N/A
Deposited data		
Original data	This paper; Mendeley Data	https://dx.doi.org/10.17632/xfwfyv74pr.1
Software and algorithms		
MATLAB	Mathworks	https://www.mathworks.com/products/MATLAB.html; RRID: SCR_001622
Simulation codes	This paper; GitHub	https://github.com/TomohikoTakei/kalman_lqg_pertpost1dof
Other		
NHP Kinarm Exoskeleton Lab	Kinarm	https://kinarm.com/kinarm-products/nhp-kinarm-exoskeleton-lab/
Plexon MAP Data Acquisition system	Plexon	https://plexon.com/products/map-data-acquisition-system-plexon/
Delsys Bagnoli	Delsys	https://delsys.com/bagnoli/

RESOURCE AVAILABILITY

Lead contact

Further information and requests for resources and reagents should be directed to and will be fulfilled by the Lead Contact, Tomohiko Takei (takeitomohiko@gmail.com).

Materials availability

This study did not generate new unique reagents.

Data and code availability

The primary datasets and simulation codes used in the current study are available at Mendely (https://dx.doi.org/10.17632/xfwfyv74pr.1) and GitHub (https://github.com/TomohikoTakei/kalman_lqg_pertpost1dof).

EXPERIMENTAL MODEL AND SUBJECT DETAILS

Subjects and apparatus

Two male rhesus monkeys (Macaca mulatta, 10–17 kg, monkeys A and R) were used in this study following procedures approved by the Queen's University Animal Care Committee. They were trained to perform upper limb motor tasks with their left arm while wearing a robotic upper-limb exoskeleton (NHP Kinarm Exoskeleton Lab; Kinarm, Kingston, Ontario, Canada) that permitted and monitored horizontal shoulder and elbow motion.[82] A virtual reality system presented visual targets and a cursor representing hand position in the workspace while direct view of their limb was occluded.

METHOD DETAILS

Behavioral task

We trained monkeys to perform a posture perturbation task, which has been described previously.[83] In the task, the monkey was required to maintain a small cursor (0.2 cm radius) representing the position of the index fingertip at a visual target (0.6 cm radius) displayed near the center of the arm's workspace (~30° and 90° degrees at the shoulder and elbow joints, respectively) (Figure 2C). The monkeys initiated each trial by moving their hand to the visual target and maintaining it within the target's acceptance window for 0.5 to 2.5 s (monkey A) or from 0.5 to 1.25 s (monkey R). The size of the acceptance window was individually adjusted to each monkey (0.8 and 1.0 cm radius for monkey A and R, respectively). Then, one of three mechanical loads was applied to the monkeys' arm. The load conditions included shoulder extension and elbow flexion (SE+EF), shoulder flexion and elbow extension (SF+EE), and an unloaded condition (catch trials). These loads stayed until the end of the trial (a step-torque perturbation) and the monkeys were required to counter the load to return to the target within 0.5 s and maintain it there for another 3.0 s (monkey A) or 2.0 s (monkey R) to receive a liquid reward. Shoulder and elbow torques of magnitude 0.28 Nm (monkey A) or 0.20 Nm (monkey R) were used. Each block consisted of four SE+EF trials, four SF+EE trials and one catch trial in random order (total nine trials per block). To mitigate the contribution of visual feedback for the rapid motor responses, we removed the hand cursor feedback for 200 ms after perturbation onset.

Cortical Cooling

After behavioral training was complete, we performed surgical procedures to implant two cooling probes over PMd and A5 as well as a head fixation post. In monkey A, we also made a craniotomy over M1 and implanted a recording chamber to record the temperature of M1. The surgeries were performed using isoflurane anesthesia (1.0%–2.0% in O2) and under aseptic conditions. PMd and A5 locations were identified based on sulcus structures on the cortical surface according to a previous electrophysiological study.[84] PMd probe was implanted between upper limb of arcuate sulcus and superior precentral sulcus, whereas A5 probe was implanted between intraparietal sulcus and postcentral dimple (Figure 2A).

Cooling probes were made with 23G stainless-steel tubing in 3 × 5 mm dimension.[19] A thermocouple is attached to the tip of the probe to monitor probe temperature. By circulating chilled methanol, the probe temperature was controlled at the desired temperature. Previous work has shown that cooling the probe to 1°C deactivates cortex up to a distance of 1.5 mm, which covers most of the cortical layers.[19] Thus, the estimated volume of deactivated cortical tissue is 72–126 mm^3.

Experimental procedure

On each experimental day, one of the cooling conditions was chosen. In experiment 1, one of the probes (PMd and A5) was cooled or no cooling was applied (sham). In experiment 2, PMd and A5 was simultaneously cooled (dual cooling). In experiment 3, PMd in monkey R was cooled to a milder target temperature (8 ± 1°C in probe temperature) instead of 0 – 1°C (milder cooling).

Each experiment was initiated with a brief practice set (3 and 2 blocks of trials for monkey A and R, respectively) with a normal acceptance window (0.8 and 1.0 cm radius for monkey A and R). After that, the pre-cooling epoch started (Figure 2B). In the pre-cooling epoch, the monkeys performed 6 (monkey A) or 3 blocks (monkey R) of trials, which consisted of 48 or 24 perturbed trials and 6 or 3 catch trials, respectively. Since we expected a motor impairment during cooling, we relaxed the acceptance window to 1.8 and 2.0 cm radius (monkey A and R) and we used the same window during all epochs (pre-cool, cool and post-cool) except for the initial practice set.

After the pre-cooling epoch, we started to circulate chilled methanol through the cooling probes and manually controlled the flow to keep the probe temperatures at the target temperature (0 – 1°C for experiment 1 and 2 and 8 ± 1°C for experiment 3). It took 80 ± 39 s to reach the target temperature (0 – 1°C). After that, we waited ~5 min for the temperatures to become stable. Then we collected behavioral data in the cooling epoch. In the cooling epoch, the monkeys performed 9 (monkey A) or 5 – 6 blocks (monkey R), which consisted of 72 or 40 – 48 perturbed trials and 9 or 5 – 6 catch trials, respectively. It took ~20 min to complete all blocks.

Then, methanol circulation was stopped and after ~5 min the post-cooling epoch started. It took 126 ± 45 s for the temperature to return back to normal (> 36°C). In the post-cooling epoch, the monkeys performed 9 (monkey A) or 5 – 6 blocks (monkey R), which consisted of 72 or 40 – 48 perturbed trials and 9 or 5 – 6 catch trials, respectively. In some recording sessions (9/94 sessions), monkey R did not complete the post-cooling epoch and we included only pre-cool and cool epoch data. We verified that inclusion of these incomplete sessions did not qualitatively affect the cooling results.

QUANTIFICATION AND STATISTICAL ANALYSIS

Data analyses

All subsequent analyses were performed offline using MATLAB (MathWorks, Natick, MA, USA).

Kinematics analyses

Kinematic data and applied torques were acquired directly by the Kinarm device and were sampled at 4000 Hz with Plexon MAP Data Acquisition system (Plexon Inc., Dallas TX, USA) and low-pass filtered (6th order double-pass filter, cutoff = 10Hz). We quantified four behavioral measurements related to spatial accuracy and response speed of the mechanical perturbation (Figure 2D).

Endpoint error was quantified to measure spatial accuracy of the feedback response. First, we identified the endpoint of the initial corrective response after the perturbation. To do this, we calculated radial hand velocity relative to the center of the target and identified the timing of the maximum inward (i.e., returning) velocity. After this time point, we sought the first timing when the monkey's hand had stopped moving according to a two-threshold method:[85] (1) the first local minimum in hand speed below 0.05 m/s or (2) when hand speed dropped below 0.005 m/s (endpoint, Figure 2D, square). Endpoint error was measured as a distance between hand position at the endpoint and the center of the target.

Return time was measured as the time interval from perturbation onset to when the hand cursor reentered the target area. Practically, we used a larger acceptance window (1.8 and 2.0 cm for monkey A and R) to keep animals rewarded even with motor impairments. However, when we calculated the return time, we used the original target size (0.8 and 1.0 cm for monkey A and R) that the monkeys were trained with (Figure 2D, circle).

Max deviation was defined as the peak hand displacement from the pre-perturbation hand position (Figure 2D, triangle). Pre-perturbation hand position was calculated as the averaged hand position during an interval from 100 to 0 ms before perturbation onset. Max deviation time is the time when max deviation occurred relative to perturbation onset.

Modulation of behavioral measures was tested by using a two-way ANOVA (cooling epochs × target areas, $p < 0.05$). As post hoc analyses, Welch's t tests were performed to compare between cooling and sham conditions ($p < 0.05$ with Bonferroni correction). Since we verified the difference of torque directions (SE+EF or SF+EE) did not qualitatively affect cooling results, we pooled the data into one dataset.

Sample size selection

After we collected the data from the first animal (monkey A), we estimated a sample size that was required for a statistical test (t test) between sham and each cooling condition to have a power of $(1 - \beta) = 0.90$ with a significance level of $\alpha = 0.01$. This calculation was done with the SAMPSIZEPWR function of MATLAB. The mean and standard deviation of the null hypothesis was set to those of the sham condition and the sample size was estimated for endpoint error, which showed significant impairment in both PMd and A5 cooling (Figure 3C). Results showed that the optimal sample size was 9 and 11 sessions for PMd and A5 cooling. Given the high variability of behaviors between animals, we set a minimal sample size for the second animal to 10 sessions for each condition.

EMG analyses

In some recording sessions (n = 33 and 58 in monkey A and R, respectively), electromyographic (EMG) activity was recorded from upper-limb muscles by attaching surface EMG electrodes over each muscle belly (Delsys Bagnoli, Delsys, Natwick MA, USA). Muscles were selected that predominantly contributed to flexion and extension movements at the shoulder and elbow (biceps, brachioradialis, brachialis, long/lateral triceps, anterior/middle/posterior deltoid, pectoralis major).[86] Muscle activity was recorded at 4000 Hz, band-bass filtered (25-350Hz, 6th order Butterworth), full-wave rectified and downsampled to 1000 Hz before analysis.

EMG signals were aligned to perturbation onset and averaged across trials. Preferred torque direction (PTD) of each EMG was determined as the torque combination (SE+EF or SF+EE) that produced the larger response in a time window from 50 to 100 ms after perturbation onset. We identified EMG as perturbation responsive if the EMG response (50 – 100 ms after perturbation) in the PTD was significantly higher than that in an unloaded catch condition (t test, $p < 0.05$). In total, we identified 293 EMG samples (n = 165 and 128 in monkey A and R) to be perturbation responsive and analyzed further (n = 140, 90 and 63 in sham, PMd and A5 cooling conditions, respectively).

EMG traces were first normalized by their mean activity during the last 2 s of the trials when the monkey was countering the load in the PTD. This normalization value was calculated with data only from the pre-cool epoch, and then the same value was applied to all EMG data in the pre-cool, cool and post-cool epochs. Then, we averaged the normalized EMG traces across muscles separately for each cooling condition. From our pilot observation, we found that EMG signals had much higher noise than kinematic signals. Therefore, we performed a selection process of the EMG data based on the behavioral effects of cooling. Our behavioral analyses showed both PMd and A5 cooling increased endpoint errors (Figure 3C). Therefore, we selected EMG data in sessions when the endpoint error was higher than the 90th percentile of the endpoint error from sham conditions. As a result, we selected 64 out of 153 EMG datasets (33 / 90 and 31 / 63 for PMd and A5 cooling). Importantly, we only used endpoint error for the selection and we used the same criteria for PMd cooling and A5 cooling. For the sham cooling data, no selection was applied (n = 140).

Muscle activity was compared across predefined epochs (baseline, 100-0 ms before perturbation onset; R1, 20-50 ms post-perturbation; R2, 50-75 ms post-perturbation; R3, 75-120 ms post-perturbation; voluntary 120-180 ms post-perturbation).[81,87] Welch's t test was used to evaluate whether the binned muscle activity was significantly modulated from sham condition ($p <$ 0.05 with Bonferroni correction).

Temperature measurement in M1

In order to evaluate the change of M1 temperature during PMd cooling sessions, we recorded intracortical temperature of M1 on PMd cooling (n = 2) or dual cooling of PMd and A5 (n = 1) sessions. Prior to the temperature recording, we mapped the arm area of M1 using intracortical microstimulation (11 pulses, 333 Hz, 0.2 ms pulse width, $\leq 20\mu A$). In each recording day, we inserted a thermocouple (HYP0-33-1-T-G-60-SMPW-M, Omega Engineering Inc, CT, USA) into the arm area of M1. We then started the experimental procedure to collect pre-cool, cool and post-cool epochs. The temperatures were sampled at 4000 Hz along with the kinematic signals.

Mean temperature during pre-cool (for 5 min before cooling onset) and cool (for 5 min before cooling offset) epochs were compared in M1 and PMd (probe temperature) separately (Figure 4). Significant modulation of temperature was evaluated with paired t test ($p < 0.05$ with Bonferroni correction).

Model simulation

We used an optimal feedback control (OFC) model developed in our previous report.[10] We considered the translation of a single-point mass (m = 1 kg) in one dimension. The control system was described by the following differential equations:

$$m\ddot{p} = -G\dot{p} + F_{ctrl} + F_{ext}$$

$$\tau\dot{F}_{ctrl} = u - F_{ctrl}$$

where m is mass, $p(t)$ is the position of the point mass as a function of time (t), G is the viscous constant, F_{ctrl} and F_{ext} are the control and external forces, respectively, u is the motor command and τ is the time constant of the linear filter for the motor command. Each trial began with F_{ext} set to 0 Nm (no external load) and after 500ms F_{ext} was suddenly changed to +2 Nm and maintained for another 1000 ms until the end of the trial (a step-torque perturbation). G was set to 1 $N \cdot s \cdot m^{-1}$, and τ was set to 40 ms, which is compatible with the first approximation of muscle dynamics.[88] Stochastic dynamics and noise disturbances are described in a discrete time system with a 10-ms time step:

$$x_{k+1} = Ax_k + Bu_k + \text{motor noise}$$

where x_{k+1} is the state vector at time $k+1$, A and B are matrices that describe the system dynamics, and u_k is the motor command at time k. Motor noise is a signal dependent Gaussian noise with variance of $(0.125)^2 \times u^6$. The state vector is represented with the four-dimensional vector,

$$x_k = [p(k)\ \dot{p}(k)\ F_{ctrl}(k)\ F_{ext}(k)]^\top$$

which was augmented with previous states to take feedback delays into account.[89] The feedback delay was set to 50 ms (5 time steps) to reflect the transcortical feedback loop delay of the long-latency response.[38] This resulted in the augmented state vector with 24 dimensions.

The feedback signal at each time step (y_k) can be written as,

$$y_{k+1} = Hx_k + \text{sensory noise}$$

where H is the observation matrix, which allows the system to observe only the most delayed state (50ms before). Otherwise, the system is fully observable. Sensory noise is an additive Gaussian noise with variance 10^{-10}. To compensate the time delay of the feedback signal, the OFC model includes an optimal linear state estimator (Kalman filter) that consists in weighting prior beliefs about the next state of the system with sensory feedback to derive a maximum likelihood estimate of the system state. Let $\hat{x}_k$ be the estimated state at time k. The prior belief about the next state (x^*_{k+1}) is defined as

$$x^*_{k+1} = \hat{A}\hat{x}_k + \hat{B}u_k + \text{prediction noise}$$

where $\hat{A}$ and $\hat{B}$ are the internal model of the system dynamics, A and B. Prediction noise is an additive Gaussian noise with variance 10^{-8}. Then, the feedback correction yields the state estimation by taking y_{k+1} into account as

$$\hat{x}_{k+1} = x^*_{k+1} + K_{k+1}\left(y_{k+1} - \hat{H}x^*_{k+1}\right)$$

where K_{k+1} is the Kalman gain at time $k+1$ and $\hat{H}$ is the internal model of the observation matrix, H. Finally, the feedback control policy is defined as

$$u_k = -L_k\hat{x}_k$$

where L_k represents the optimal feedback gain at time k.

The cost function for the task was defined as:

$$J = \sum_{t=1} q_p(t)p(t)^2 + q_v(t)\dot{p}(t)^2 + ru(t)^2$$

where J is the total-cost including error cost (position and velocity) and motor cost over a time-course of the trial. q_p and q_v are time-dependent factors which define the cost of position and velocity errors, respectively. Both were set to 1 before and 500 ms after the perturbation, but they were set to 0 between 0 and 500 ms after the perturbation. This means that the model is required to stay at (p, $\dot{p}$) = (0, 0) except for just after the perturbation. r is a constant factor which defines the cost of control and it was set to 10^{-6}.

With these definitions of the system dynamics, feedback signals, noise parameters, and cost functions, we computed the optimal feedback gains (L) and Kalman gains (K) following algorithms adapted for the presence of signal-dependent noise.[23,89]

Simulation for cortical deactivations

To apply deactivation of the optimized model parameters, we used two different methods: downscaling and noise addition. For downscaling, we multiply a scalar between 0 – 1 to deactivate the parameter. For example, when we deactivate a parameter by 20%, we multiply 0.8 (= 1 – 0.2) to the optimized value of the parameter. The rational of this method is that cortical cooling is known to reduce neural excitability at mainly post-synaptic terminals,[90] suggesting that cooling reduced the gain to the pre-synaptic inputs. Another possibility is that cortical cooling adds some noise to the neural computations by affecting the balance of excitatory and inhibitory neural activity. To replicate this scenario, we added scaled Gaussian noise to the target parameters. To control for manipulation size, the noise was chosen from a normal distribution whose standard deviation was scaled with the absolute value of each parameter:

$$noise \sim N(0, \alpha|x|)$$

where $|x|$ is absolute of the optimal value for the target parameter and α is a scaling factor of added noise chosen from 0 to 1. This means that noise size was normalized to the coefficient of variation (CV): $\alpha = 0$ indicates that no noise was added (0% CV), whereas $\alpha = 1$ indicates that noise chosen from normal distribution with standard deviation of $|x|$ (100% CV). Once noise was selected for each parameter in each simulation repeat, the value was fixed and not changed during a trial time course.

With either deactivation method, we applied deactivation to each target parameter and evaluated the behavioral measures with the same algorithms used for the monkey behavioral analyses (Figure 2D). Then we applied a two-way ANOVA (deactivation size × deactivated parameters) and post hoc paired t tests to evaluate whether the behavioral measures were modulated from the optimal conditions ($p < 0.05$ with Bonferroni correction). Deactivation size for downscaling was chosen from 0 – 100% with a 5% step size, whereas deactivation size for noise addition was chosen from 0 – 40% with a 2% step size.